DOI: 10.1021/ma1020352

Macromolecules
ARTICLE

Local Relaxation Behavior and Dynamic Fragility in Hydrogen Bonded Polymer Blends

Kevin A. Masser, Hanqing Zhao, Paul C. Painter, and James Runt*

Department of Materials Science and Engineering, The Pennsylvania State University, University Park, Pennsylvania 16802, United States

Received September 1, 2010; Revised Manuscript Received October 1, 2010

ABSTRACT: The dynamics of intermolecularly hydrogen-bonded polymer blends of poly(*p*-(hexafluoro-2-hydroxyl-2-propyl)styrene) with poly(vinyl acetate), poly(ethylene[30]-*co*-vinyl acetate[70]) and poly(ethylene-[55]-*co*-vinyl acetate[45]) are investigated by broadband dielectric relaxation spectroscopy and Fourier transform infrared spectroscopy. Each blend component exhibits a glassy state (β) relaxation, and these relaxations are affected by the formation of intermolecular associations. The glassy state behavior of the blends can be modeled using the Painter−Coleman association model. All blends exhibit a single T_g and a single dielectric segmental (α) relaxation, indicative of strong segmental-level coupling. The fragility of the glass-formers depends on the volume fraction of intermolecularly associated segments, and the association model predicts which compositions have the highest fragilities. A relaxation related to the breaking and reforming of hydrogen bonds is observed at temperatures above the α process, and its temperature dependence varies systematically with ethylene content.

Introduction

Most miscible polymer blends in which the components do not form specific intermolecular interactions are now well-known to exhibit two segmental (α) relaxations or glass transition temperatures (T_g) when the difference in component T_g's (ΔT_g) is greater than ~50 °C. Notable exceptions to this are blends of high molecular weight polymers with oligomers of the same repeat unit, exhibiting a single T_g with a large disparity between the component T_g's.[1] Chain connectivity effects[2] result in concentration fluctuations and the compositional dependence of the two T_g's or α processes can generally be described by the Lodge−McLeish model.[3−5] Painter and Coleman introduced an additional "chemical forces" term ($\Delta G_H/RT$) to the Flory−Huggins equation to account for the free energy change due to hydrogen bonding (typically having energies of 4−42 kJ/mol).[6] The presence of sufficient intermolecular hydrogen bonding between component polymers in a binary mixture leads to coupling of motions on the molecular level, and typically result in a single T_g and a single segmental (α) relaxation, even when ΔT_g is 100 °C or larger.

In our earlier studies of miscible poly(4-vinylphenol) (PVPh) blends, despite the presence of strong hydrogen bonding between the component polymers, two α relaxations are observed at the compositional extremes.[7−9] This arises due to a stoichiometric effect, exacerbated by the strong self-associations (OH−OH hydrogen bonds) formed between PVPh segments. To reduce self-associations, Painter, Coleman, and co-workers used selective steric shielding around the OH functionality.[10−12] The steric shielding serves to limit the ability of two such functional groups forming a hydrogen bond, while not appreciably reducing the OH-containing species' ability to form a hydrogen bond with a proton acceptor such as poly(vinyl methyl ether) (PVME). Shown in Figure 1 are the repeat unit structures of the (co)polymers used in this study. The two CF_3 groups of poly(1,1,1,3,3,3-hexafluoro-2-(4-vinylphenyl)propan-2-ol) (PolyHFS) provide steric shielding which reduces the ability to form self-associations.

*To whom correspondence should be addressed. E-mail: runt@matse.psu.edu.

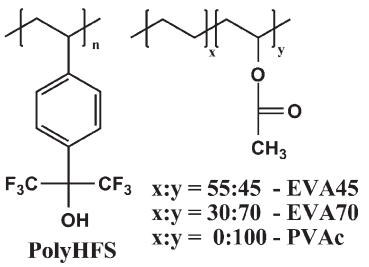

Figure 1. Repeat units of the polymers used in this study.

The wavenumber shift of the OH band in Fourier transform infrared (FTIR) spectroscopy has been shown to be an indicator of hydrogen bonding strength.[6,10] In blends of PVPh with PVME, for example, the wavenumber difference between PVPh self-associations and intermolecular associations with PVME is less than ~50 cm^{-1} greater than the PVPh self-associations, meaning that intermolecular associations are only slightly more thermodynamically favorable. In analogous PolyHFS blends with PVME,[13] the wavenumber difference between HFS self-associations and PVME intermolecular associations is approximately 320 cm^{-1}, underlying the importance of reduced self-associations.

The association model has been found to accurately predict phase behavior rather well.[6,14] Knowledge of the equilibrium constants for forming OH−OH bonds (K_2), OH multimers (K_B), OH-carbonyl intermolecular bonds in the present case (K_A) and molar volumes of the blend components, allows for the calculation of the phase behavior and the fractions of hydrogen-bonded species present as a function of composition. Knowledge of the hydrogen bonding enthalpies is necessary to calculate the phase behavior at any temperature.

The carbonyl region of the FTIR spectrum (~1650−1800 cm^{-1}) is sensitive to hydrogen bonding. An additional band, shifted to lower wavenumber relative to the nonbonded carbonyl absorbance, appears when carbonyl groups participate in a hydrogen bond. This region of the FTIR spectrum is readily modeled

 Published on Web 10/13/2010

Table 1. Thermal Characteristics of the Blends Studied

blend	mol % HFS (±1%)	wt % HFS (±1%)	T_g (±3 °C)
PVAc	0	0	41
	10	25	49
	24	50	65
	49	75	109
	74	90	122
	100	100	125
EVA70	0	0	−10
	13	25	2
	31	50	24
	58	75	86
	80	90	100
EVA45	0	0	−24
	19	25	−12
	41	50	17
	68	75	72
	86	90	75

compared to the OH region,[15,16] yielding quantitative information on the fraction of hydrogen-bonded segments. The obtained fraction of free carbonyl groups from a series of blend compositions can be fit to the stoichiometric equations of the association model, yielding the various equilibrium constants.[6,10]

In the current investigation, we use these stoichiometric equations to predict the number and types of hydrogen bonding species present in a series of blends of PolyHFS with ethylene-vinyl acetate copolymers. Using information determined by curve-resolving the carbonyl region of FTIR spectra, we are able to describe the glassy state relaxations of these systems, as well as predict which compositions should have the highest fragility. To the authors' knowledge, this has not been demonstrated previously, and this methodology should be applicable to any miscible blend in which the hydrogen bonding behavior can be quantified.

Experimental Section

The (co)polymers poly(vinyl acetate) (PVAc), poly(ethylene-[30]-*co*-vinyl acetate[70]) (EVA70), and poly(ethylene[55]-*co*-vinyl acetate[45]) (EVA45) were purchased from Scientific Polymer Products and have molecular weights of approximately 100 kg/mol. Note that the numbers in brackets refer to the weight % of each component. Each was dissolved in a good solvent, passed through a 0.2 μm Teflon syringe filter, then reprecipitated into hexanes. The precipitate was collected and dried well above T_g prior to use. Synthesis of PolyHFS ($\overline{M_W}$ = 140 kg/mol, PDI = 1.4) is described in a previous publication.[13] As with the other polymers, it was filtered and reprecipitated prior to use.

Blend Preparation. Appropriate amounts (see Table 1) of each component were added to a Teflon jar along with an appropriate good solvent. For the PVAc blends, acetone was used. For the EVA70 blends, a mixture of 70 vol % tetrahydrofuran (45 vol % for the EVA45 blends) with toluene was used. After dissolving each component, the solution was passed through a 0.2 μm Teflon syringe filter. Each solution was stirred for approximately 20 h, after which an air purge was added to remove the solvent. All blends were then dried at approximately 150 °C for at least 12 h with a liquid nitrogen trap under vacuum (2−3 μbar) to remove solvent and moisture.

Differential Scanning Calorimetry (DSC). Thermal characteristics were measured using a Seiko DSC220CU DSC. Samples for DSC measurements were cut from the dried blend film and crimped in aluminum pans. Each sample was scanned using the following procedure: Heat at 10°/min to T_g + 50 °C, cool at 10°/min to T_g − 50 °C, heat to T_g + 50 °C at 10°/min. The temperature was held for 5 min at each extreme (T_g ± 50 °C) before continuing. T_g was taken from the second heating as the midpoint of the heat capacity change.

Fourier Transform Infrared Spectroscopy (FTIR). Spectra were collected on a Nicolet 6700 with an attached dry air purge. A minimum of 100 scans were averaged with a wavenumber resolution of 1 cm^{-1}. Samples were cast from a good solvent (see above) onto potassium bromide windows, then dried at 150 °C overnight under vacuum (2−3 μbar). Film thickness was controlled such that the absorbance was within the range of the Beer−Lambert law.

Curve resolving was performed on the carbonyl region of the spectra (1700−1750 cm^{-1}) using a fitting program developed at Penn State.[6] Peaks were modeled with two Gaussian functions:[17]

$$I(\nu) = A_o \exp\left[-\ln 2\left[\frac{\nu-\nu_o}{\Delta\nu_{1/2}}\right]^2\right] \quad (1)$$

$\Delta\nu_{1/2}$ is the half width at half height, ν_o is the wavenumber coordinate of the band maximum, and ν is the frequency.

Calculations of Hydrogen Bond Types. The hydrogen bond stoichiometry in the blends was calculated using the Painter−Coleman association model.[6,18] The volume fractions (ϕ) of the two polymers can be described by:

$$\phi_A = \phi_{A_1} + K_A\phi_{A_1}\phi_{B_1}\Gamma_1 \quad (2)$$

$$\phi_B = \phi_{B_1}\Gamma_2\left[1+\frac{K_A\phi_{A_1}}{r}\right] \quad (3)$$

ϕ_{A_1} and ϕ_{B_1} are the volume fractions of free (nonbonded) A and B segments, respectively, and r is the ratio of the molar volumes of A and B. Γ_1 and Γ_2 are given by:

$$\Gamma_1 = \left[1-\frac{K_2}{K_B}\right] + \frac{K_2}{K_B}[1-K_B\phi_{B_1}]^{-1} \quad (4)$$

$$\Gamma_2 = \left[1-\frac{K_2}{K_B}\right] + \frac{K_2}{K_B}[1-K_B\phi_{B_1}]^{-2} \quad (5)$$

K_2, K_A, and K_B were determined for the systems under investigation here by Yang et al.[10] The fraction of hydrogen-bonded A (vinyl acetate) and B (HFS) groups can then be calculated using eqs 6 and 7, respectively.

$$f_{HA} = 1-\frac{\phi_{A_1}}{\phi_A} \quad (6)$$

$$f_{HB} = 1-\frac{\Gamma_1}{\Gamma_2}\left[1+\frac{K_A\phi_{A_1}}{r}\right]^{-1} \quad (7)$$

The fraction of free HFS groups, (f_F^{OH}) is simply $1 - f_{HB}$. The fraction of free carbonyl groups ($f_F^{C=O}$) is ($1 - f_{HA}$) or:

$$f_F^{C=O} = \frac{\phi_{A_1}}{\phi_A} = \left\{1+K_A\phi_{B_1}\left[\left(1-\frac{K_2}{K_B}\right)+\frac{K_2}{K_B}(1-K_B\phi_{B_1})^{-1}\right]\right\}^{-1} \quad (8)$$

Since PolyHFS forms self-associations as well as intermolecular associations, an additional term to account for the fraction of these self-associations is necessary. The fraction of self-associated HFS segments (f_B^{OH-OH}) is related to the volume fraction of self-associated B groups (ϕ_{B_n}) by:

$$f_B^{OH-OH} = \frac{\sum_{n=2}^{\infty}\phi_{B_n}}{\phi_B} = \frac{\frac{K_2}{K_B}[(1-K_B\phi_{B_1})^{-2}-1]}{\Gamma_2} \quad (9)$$

Note that these calculations are for the state of hydrogen bonding at room temperature (25 °C), and the hydrogen bonding

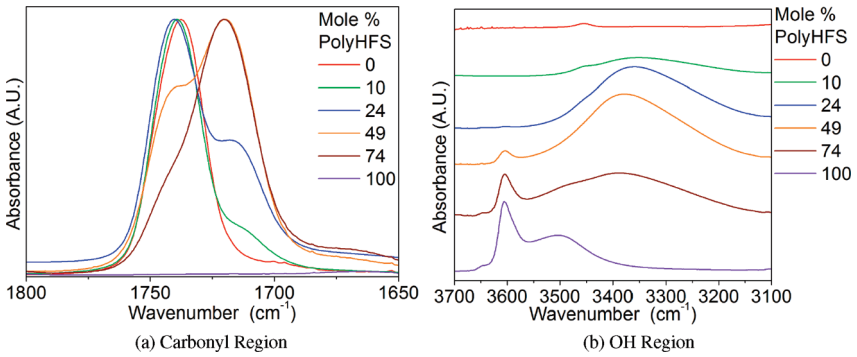

Figure 2. Scaled FTIR results for the PVAc blends with PolyHFS. The carbonyl (a) and OH regions (b) are shown. Data in part b are vertically offset for clarity.

behavior depends on temperature. The enthalpies of hydrogen bond formation, which are currently unknown for these systems, would be required to evaluate the hydrogen bonding behavior at temperatures other than 25 °C.

Broadband Dielectric Relaxation Spectroscopy (DRS). Samples were prepared for DRS measurements by solution casting thin films, typically 60−70 μm thick, from a good solvent (see above) directly onto brass electrodes, 20−30 mm in diameter. A smaller diameter upper electrode was pressed into the film along with two 50 μm diameter silica spacers to maintain sample thickness. Each sample was dried under vacuum (2−3 μbar) at high temperatures prior to measurement, and samples were transferred from the oven after cooling to room temperature to the spectrometer as quickly as possible. The effects of water on glassy state dynamics are well-known.[19,20] Water is known to alter the relaxation behavior of not only the local relaxation of PVAc,[21] but also the segmental relaxation,[22] so great care was taken to minimize the sample exposure to moisture.

DRS measurements were performed on a Concept 40 system from Novocontrol GmbH, and measured over the frequency range 10 mHz to 10 MHz. Temperature was controlled by a Quatro temperature control system with a precision of greater than ±0.1 °C. All blends were measured over the temperature range from −140 °C to well above the calorimetric T_g. After DRS measurements, films were redissolved in good solvent to ensure that cross-linking did not occur at elevated temperatures.

The imaginary part (loss) of the complex dielectric function ($\varepsilon^*(\omega) = \varepsilon'(\omega) - i\varepsilon''(\omega)$) was fit using one or more empirical Havriliak−Negami (HN) equations:[23]

$$\varepsilon''(\omega) = -\sum_{r=1}^{z} \mathrm{Im}\frac{\Delta\varepsilon_r}{(1+(i\omega\tau_{HNr})^{a_r})^{b_r}} + \frac{\sigma_o}{\varepsilon_o\omega^s} \qquad (10)$$

$\Delta\varepsilon_r$ is the strength of the relaxation, and is related to the number of dipoles contributing to the dispersion.[24−26] ω and τ_{HNr} are the angular frequency and relaxation time, respectively. a_r and b_r are the broadening and high frequency asymmetry parameters, respectively. The second term of equation eq 10 describes the dc conductivity, a result of motions of impurity ions. σ_o is the frequency-independent (dc) conductivity, ε_o is the permittivity of free space, and the parameter s relates to the type of conduction present.[26]

At temperatures above T_g, the motions of impurity ions begin to dominate the dielectric loss, often obscuring dipolar relaxations. With the exception of the phenomenon of electrode polarization, motions of ionic impurities are not manifested in the dielectric constant (ε').[26] The fundamental Kramers−Kronig relationship states the dielectric loss and the dielectric constant contain the same information, so one can be calculated from the other. Since a cumbersome numerical approximation is necessary for the Kramers−Kronig relationship to be applied,[27] the derivative of the dielectric constant was used. Wübbenhorst et al. have shown that the derivative of the dielectric constant is a good approximation of the 'conductivity-free' dielectric loss:[28,29]

$$\varepsilon_D'' = -\frac{\pi}{2}\frac{\partial\varepsilon'(\omega)}{\partial(\ln\omega)} \approx \varepsilon'' \qquad (11)$$

The usefulness of this formalism is its ability to not only remove dc conductivity from the dielectric loss, but it has also been shown to partially resolve overlapping peaks.[30] As long as the appropriate fitting function is used in the analysis of the data, the derivative formalism yields results identical to the raw dielectric loss, with the added benefit of being able to deconvolute dipolar response from ion motion.[30,31] From ref 30:

$$\frac{\partial\varepsilon'(\omega)}{\partial(\ln\omega)} = -\frac{ab\Delta\varepsilon(\omega\tau_{HN})^a\cos[a\pi/2-(1+b)\theta_{HN}]}{[1+2(\omega\tau_{HN})^a\cos(a\pi/2)+(\omega\tau_{HN})^{2a}]^{(1+b)/2}} \qquad (12)$$

with

$$\theta_{HN} = \arctan\left[\frac{\sin(\pi a/2)}{(\omega\tau_{HN})^{-a}+\cos(\pi a/2)}\right] \qquad (13)$$

The parameters in eqs 12 and 13 are the same as those in eq 10.

From the relaxation time (τ_{HN}) determined by fitting eq 10 to the dielectric loss data, or eq 12 to the derivative loss, the frequency maxima can be calculated from the following:

$$f_{max} = \frac{1}{2\pi\tau_{HN}}\left[\frac{\sin\left(\frac{a\pi}{2+2b}\right)}{\sin\left(\frac{ab\pi}{2+2b}\right)}\right]^{1/a} \qquad (14)$$

Results and Discussion

DSC. A single calorimetric T_g was observed for each blend, and these are listed in Table 1 along with the blend compositions.

FTIR. Shown in Figures 2a, 2b, 3a, 3b, 4a, and 4b are the FTIR spectra (scaled by each spectra's maximum) illustrating the state of hydrogen bonding present in these blends at room temperature. As noted earlier, careful analysis of the carbonyl region of the FTIR spectra (1700−1750 cm^{-1}) allows one to obtain the fractions of free and hydrogen-bonded segments. Shown in Figure 5 is an example curve-resolved spectrum.

The carbonyl region consists of two main peaks: a "free" (non-hydrogen-bonded) band located at 1739 ± 3 cm^{-1} and a hydrogen-bonded carbonyl band centered at approximately 1713 ± 3 cm^{-1}. Two Gaussian functions were used (eq 1) in the curve-resolving, one for the 1739 cm^{-1} band and another

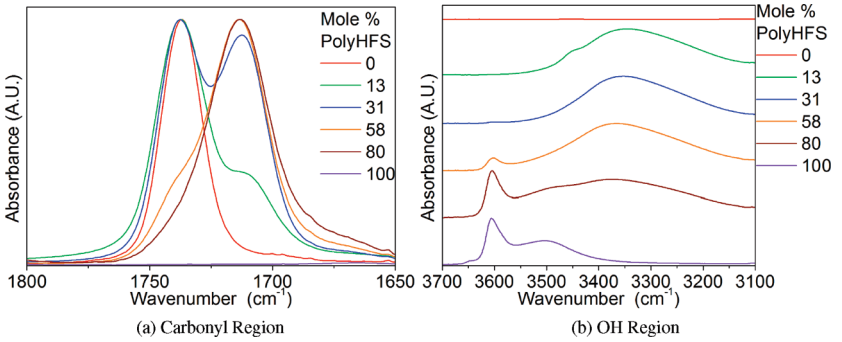

Figure 3. Scaled FTIR results for the EVA70 blends with PolyHFS. The carbonyl (a) and OH regions (b) are shown. Data in part b are vertically offset for clarity.

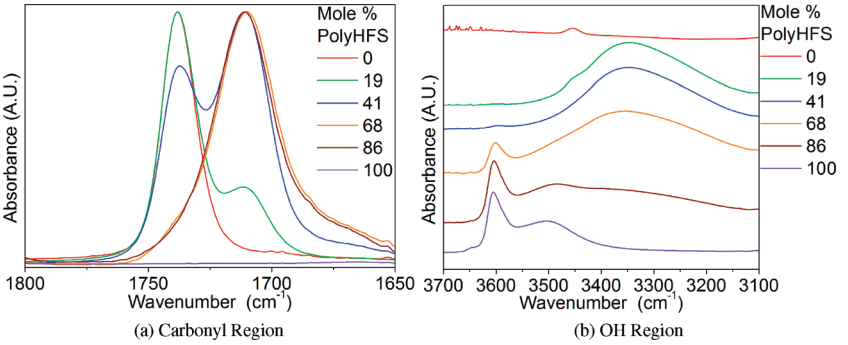

Figure 4. Scaled FTIR results for the EVA45 blends with PolyHFS. The carbonyl (a) and OH regions (b) are shown. Data in part b are vertically offset for clarity.

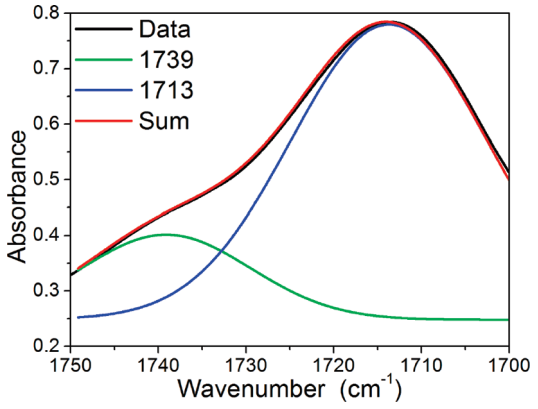

Figure 5. Representative curve-resolved FTIR spectra in the carbonyl region for the 58 mol % PolyHFS blend with EVA70.

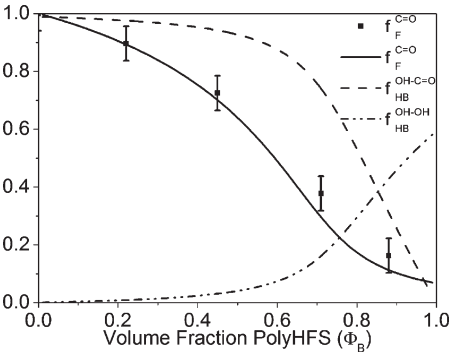

Figure 6. Composition dependence of the fraction of free carbonyl groups from the association model (solid line), fraction of intermolecularly associated HFS segments from the model (dashed line), fraction of self-associated HFS segments from the model (dash-dot line), and the experimentally determined fraction of free carbonyl groups (squares) for the PVAc blends at 25 °C.

for the 1713 cm^{-1} band, along with a linear baseline. From knowledge of the ratio of the absorptivity coefficients (free/interassociated $=1.5$),[10] one can obtain the fraction of free carbonyl groups as a function of composition.

In a previous study, the room temperature (25 °C) equilibrium association constants for the formation of an intramolecular hydrogen bond between the HFS and acetoxy functionalities ($K_A = 34.5$), as well as the self-association constants for PolyHFS (dimers $K_2 = 2.53$, and multimers $K_B = 3.41$) were determined.[10] These values, combined with knowledge of the molar volume of each segment (HFS $= 170\ cm^3/mol$, VAc $= 69.8\ cm^3/mol$, $CH_2 = 16.5\ cm^3/mol$), and eqs 2−9,[6] allow for the prediction of the amount and types of hydrogen bonding species present as a function of composition. Shown in Figures 6−8 are the fractions of free carbonyl groups determined experimentally, as well as the predicted fractions of free carbonyl groups, *inter*molecularly associated HFS segments, and *intra*molecularly associated HFS segments. At all compositions, good agreement is found between the model predictions for the fraction of free carbonyl groups and the experimental results.

Broadband Dielectric Relaxation Spectroscopy. *Local Relaxations.* The vinyl acetate functionality exhibits a well-known glassy state motion in PVAc,[21,32,33] and the experimental Arrhenius (eq 15) fit parameters for this β relaxation (frequency prefactor $f_0 = 10^{12.5}$ Hz, and activation energy $E_a = 40$ kJ/mol) agree well with the literature.[32]

$$f_{max}(T) = f_o \exp\left(-\frac{E_a}{RT}\right) \tag{15}$$

Shown in Figure 9 is an Arrhenius plot containing representative relaxation frequencies of the local relaxations observed, based on the experimentally determined relaxation

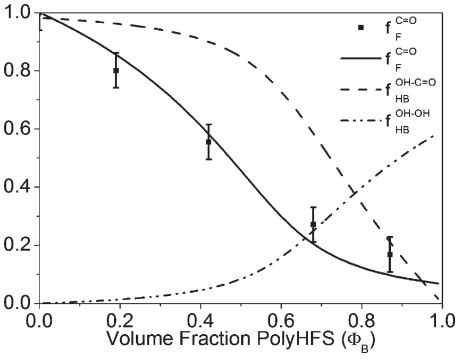

Figure 7. Composition dependence of the fraction of free carbonyl groups from the association model (solid line), fraction of intermolecularly associated HFS segments from the model (dashed line), fraction of self-associated HFS segments from the model (dash-dot line), and the experimentally determined fraction of free carbonyl groups (squares) for the EVA70 blends at 25 °C.

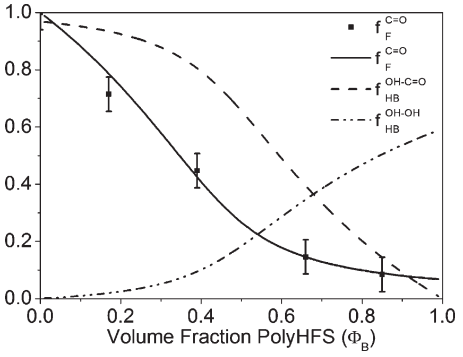

Figure 8. Composition dependence of the fraction of free carbonyl groups from the association model (solid line), fraction of intermolecularly associated HFS segments from the model (dashed line), fraction of self-associated HFS segments from the model (dash-dot line), and the experimentally determined fraction of free carbonyl groups (squares) for the EVA45 blends at 25 °C.

times. The Arrhenius fit parameters corresponding to the black lines in Figure 9 are listed in Table 2.

Both EVA70 and EVA45 exhibit a local relaxation, which, compared to the PVAc process, is shifted to lower temperatures with increasing ethylene content, in agreement with findings in the literature.[21] The vinyl acetate β relaxation maintains the same activation energy, but the Arrhenius prefactor increases from $f_0 = 10^{12.5}$ Hz for PVAc to $f_0 = 10^{15}$ Hz for EVA70, and $f_0 = 10^{15.3}$ Hz for EVA45 (see Table 2). This shift can be ascribed to the coupling of this motion to that of the main chain, as observed in neutron scattering experiments,[34] and the degree of coupling decreases with increasing ethylene content.[21] As noted in a previous study,[13] PolyHFS exhibits a β relaxation having an activation energy of 54 kJ/mol and an Arrhenius prefactor of 10^{16} Hz.

Upon blending PolyHFS with PVAc, EVA70, or EVA45, an additional relaxation appears in the glassy state, shown by the black vertical lines in Figures 10a to 10c and the orange diamonds in Figure 9. The Arrhenius fit parameters for this process, which we refer to as the β' relaxation, are $f_0 = 10^{17.2}$ Hz and $E_a = 70$ kJ/mol, both higher than those of the local processes of any of the component polymers (see orange points of Figure 9).

Inspection of parts a−c of Figure 10 reveals that the magnitude of the β' relaxation changes systematically with composition. The β' process increases in magnitude with increasing PolyHFS content, to a maximum in the 50 PolyHFS mol % blend with PVAc, the 58 PolyHFS mol % blend with

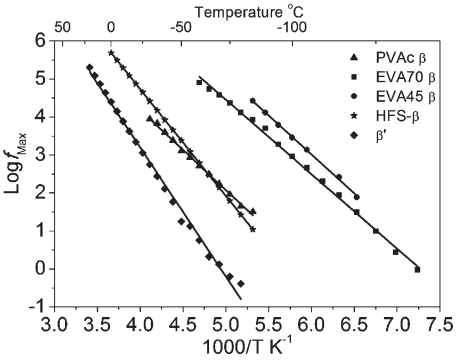

Figure 9. Arrhenius plot of the observed glassy-state relaxations. Black lines are fits to an Arrhenius function.

Table 2. Arrhenius Fit Parameters for the Local Relaxations Present in the Blends Studied

relaxation	log(f_0) (±0.1 log(Hz))	E_a (±0.5 kJ/mol)
PVAc β	12.5	40
EVA70 β	15	40
EVA45 β	15.3	40
HFS β	16	54
β'	17.2	70

EVA70, and the 68 PolyHFS mol % blend with EVA45 (orange points in Figures 10a to 10c). The strength of this process is reduced at the next highest PolyHFS composition in each blend, suggesting this process is related to the hydrogen-bonded HFS segments. Further evidence for this is found in the FTIR OH stretching region of each blend (Figures 2b, 3b, and 4b). Each of the blends at higher PolyHFS content (74, 80, and 86 mol % PolyHFS with PVAc, EVA70 and EVA45 respectively) possess not only free HFS segments, demonstrated by the band at 3602 cm^{-1}, but also self-associations (HFS−HFS bonds), shown by the broad shoulder at 3500 cm^{-1}, and an absence of free vinyl acetate groups (Figures 2a, 3a, and 4a). This demonstrates, beyond the fact that there is a large molar excess of PolyHFS at these compositions, that the majority of the HFS segments are either free or self-associating. The local response for these compositions (brown points in Figure 10a−c), should therefore be dominated by the response of HFS segments which behave as neat PolyHFS.

Using predictions of the fractions of free and hydrogen-bonded segments, and assuming the β' process arises from hydrogen-bonded HFS segments, it should be possible to fit the local processes with two HN functions (see eq 10), keeping a majority of the fit parameters fixed. Specifically, the ratio of dielectric strengths ($\Delta\varepsilon_{Free}/\Delta\varepsilon_{Bonded}$) of the hydrogen-bonded functional groups (β') and the free functional groups (HFS-β) can be calculated using the prediction lines in Figures 6−8, calculated from eq 9. $\Delta\varepsilon$ is related to the number density of dipoles participating in a relaxation,[25] so the ratio of the two dielectric strengths should be related to the fraction of segments free and hydrogen bonded. This assumes no difference in dipole moment between the free and hydrogen-bonded segments.[26] The temperature dependence of the β' relaxation is constant in all blends (PVAc, EVA70, EVA45), as is the PolyHFS β relaxation. The relaxation times ($\tau_{\beta'}$ and $\tau_{HFS-\beta}$), can therefore also be fixed, since the PolyHFS β relaxation times are determined from the homopolymer results, and the β' relaxations are determined by iteratively fitting the 12 blend compositions, with particular emphasis placed on the compositions where the β' relaxation is dominant, for instance, the 24 mol % PolyHFS blend with PVAc. Additionally, since these are glassy state relaxations,

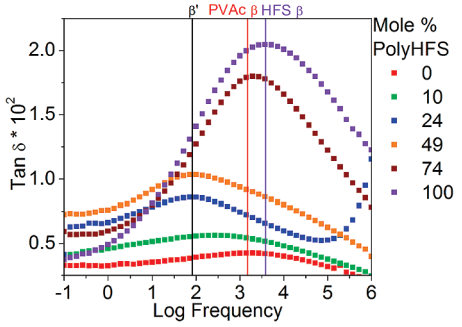

(a) PVAc Blends -50 °C

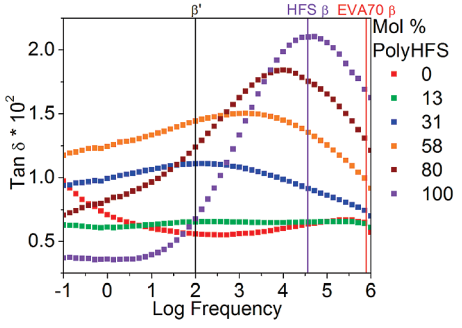

(b) EVA70 Blends -30 °C

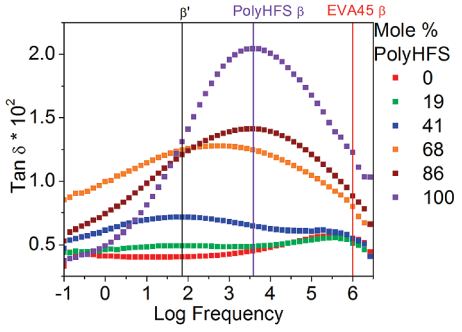

(c) EVA45 Blends -50 °C

Figure 10. Tan δ for the (a) PVAc blends at −50 °C, (b) EVA70 blends at −30 °C, and (c) EVA45 blends at −50 °C. The vertical lines mark the locations of the PolyHFS local relaxation (purple), the vinyl acetate local relaxation (red), and the β' relaxation (black).

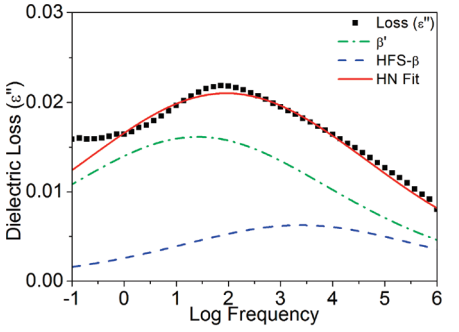

(a) 49 mol% PolyHFS with PVAc

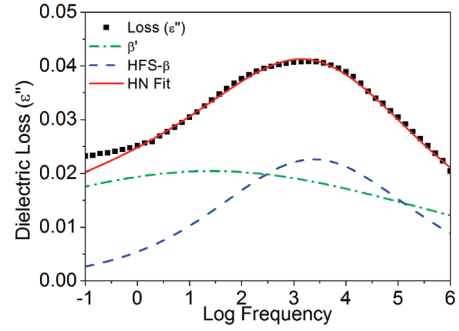

(b) 80 mol% PolyHFS with EVA70

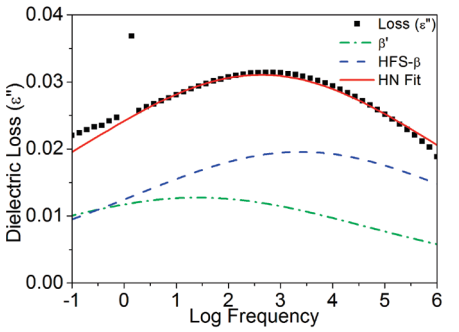

(c) 68 mol% PolyHFS with EVA45

Figure 11. Representative fits to the local relaxations in each blend at −50 °C. The ratio of dielectric strengths were calculated from the Painter−Coleman model.

the high frequency asymmetry parameters ($b_{\beta'}$ and $b_{\mathrm{HFS}-\beta}$ from eq 10 can be fixed to unity. Since these relaxations occur in the glassy state and no ion motion occurs, the second term in eq 10 is omitted. The resulting two HN fit to two relaxations uses three adjustable parameters: the relaxation breadths ($a_{\beta'}$ and $a_{\mathrm{HFS}-\beta}$) and the relationship between dielectric strengths determined from the association model prediction ($\Delta\varepsilon_{\mathrm{HFS}-\beta} = \Delta\varepsilon_{\beta'}[(1/f_{\mathrm{HB}}^{\mathrm{OH-C=O}}) - 1]$. Note that the contribution from HFS self-associations is accounted for in the $\Delta\varepsilon_{\mathrm{HFS}-\beta}$ term, since they are also present in the HFS homopolymer. The breadth parameters $a_{\mathrm{HFS}-\beta}$ and $a_{\mathrm{HFS}-\beta'}$ were restricted to within 0.1 of the "neat" relaxations, and do not change appreciably between systems.

Blends with high PolyHFS content were chosen to evaluate the validity of the above prediction, since the strength of the vinyl acetate local relaxation is small relative to that of PolyHFS, and its contribution is minimized. Making the assumption that the vinyl acetate local relaxations are negligible, two instead of three fit functions are required. Blends with free HFS segments and relatively few free carbonyl groups were chosen based on the FTIR results. Representative results of this fitting process are shown in Figure 11a−c.

This method appears to describe the data well, except at low frequencies, suggesting the β' relaxation does indeed arise from hydrogen-bonded HFS segments. Although not shown here, the agreement with the data is better at higher temperatures, particularly for the PVAc blends (Figure 11a). The lack of experimentally equilibrium constants at low temperatures may be the origin of the low frequency disagreement between the data and the prediction in Figure 11a−c. The conclusion that the β' relaxation arises from hydrogen-bonded segments is also in agreement with the higher activation energy of this process compared to the other local relaxations (see Table 2), since hydrogen bonds must be broken for this relaxation to occur. This fitting routine produced similar fits to all blends with PolyHFS compositions greater than 50 mol %. Fitting low PolyHFS content blends in a similar manner (two HN functions: one for β', one for the vinyl acetate β) is not as straightforward. The low strength of the vinyl acetate β process makes it difficult to accurately model in blends where its

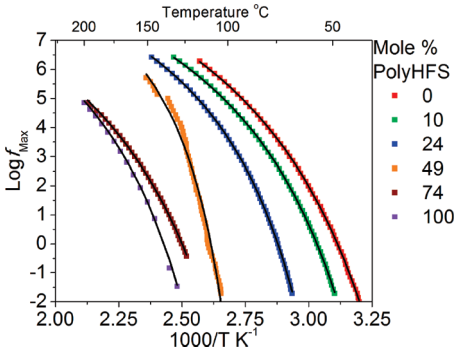

Figure 12. Segmental relaxation frequencies for the PVAc blends. Black lines are VFT fits.

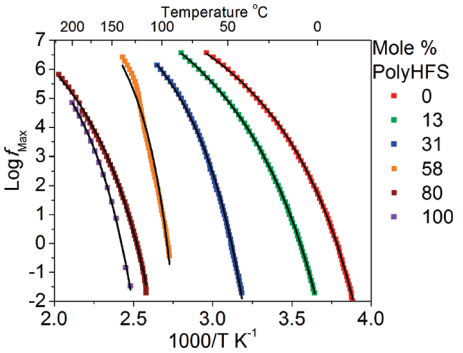

Figure 13. Segmental relaxation frequencies for the EVA70 blends. Black lines are VFT fits.

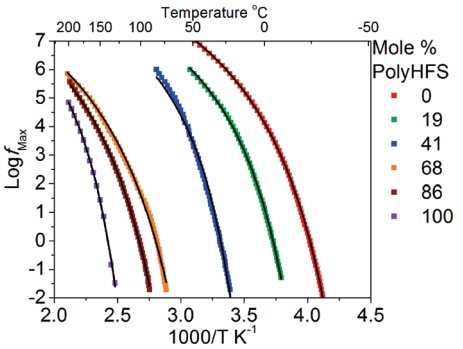

Figure 14. Segmental relaxation frequencies for the EVA45 blends. Black lines are VFT fits.

intensity is reduced from that of the neat polymer due to hydrogen bonding.

In contrast to more strongly hydrogen-bonded blends such as PVPh with poly(2-vinylpyridine) (P2VPy),[8] PVPh and PVME,[7] and PolyHFS blends with P2VPy and PVME,[13] the hydrogen bonds formed between the HFS and vinyl acetate functionalities are not sufficiently strong to completely suppress the local relaxations. As mentioned above, the wavenumber difference between the free OH band and the intermolecularly associated OH band provides a relative measure of the hydrogen bonding strength. The blends examined here exhibit an OH wavenumber shift of approximately 250 cm^{-1}, up to several hundred wavenumbers less than equivalent PVME and P2VPy blends,[13] suggesting the hydrogen bonds formed in these systems are significantly weaker than in PVME and P2VPy blends.

Segmental Relaxations. As in our previous study on blends of PolyHFS with PVME and P2VPy, all blends studied here exhibit a single segmental relaxation, indicative of segmental-level coupling, or dynamic homogeneity at this length scale, and in agreement with the miscibility predictions of the Painter−Coleman association model.[6,13] Additionally, small-angle X-ray scattering (not shown) did not reveal any structure. The segmental relaxation frequencies for the blends examined here are shown in Figures 12−14.

The temperature dependence of the segmental relaxation can be described by a Vogel−Fulcher−Tamman (VFT) equation:[26]

$$f_{\max}(T) = f_o \exp\left(-\frac{B}{(T - T_o)}\right) \qquad (16)$$

f_0 is the exponential prefactor, or the relaxation frequency at infinite temperature. B is related to the fragility of the system,[35] which can also be written as DT_0, where D is a fragility parameter.[31,36] T_0 is the Vogel temperature, or the temperature at which eq 16 diverges. The resulting VFT parameters from the fits to the curves in Figures 12-14 are listed in Table 3.

The steepness (or fragility) index of a glass former is defined as

$$m = \left.\frac{\partial(\log_{10} x)}{\partial(T_g/T)}\right|_{T=T_g} = \frac{BT_g}{\ln_{10}(T_g - T_o)^2} \qquad (17)$$

x is a dynamic variable such as viscosity (η) or relaxation time ($\tau = 1/2\pi f$) as in the case of this study.[35] A "fragile" glass former (higher value of m) is one with a greater deviation from Arrhenius behavior: one whose slope of the segmental relaxation time/frequency at $T = T_g$ is higher. Note that fragility was calculated with the VFT-determined T_g ($\tau_{max} = 100$ s), and these are also listed in Table 3.

Of particular interest is the 49 PolyHFS mol % blend with PVAc (orange points in Figure 12), the 58 PolyHFS mol % blend with EVA70 (orange points in Figure 13) and the 41 PolyHFS mol % blend with EVA45 (blue points in Figure 14). These blends have the highest fragilities (see Table 3) in each of their respective blend series. Inspection of the FTIR results reveals these blends have both the fewest free carbonyl groups and fewest free HFS segments in their respective series (demonstrated by the peak at 1737 cm^{-1} in Figures 2a, 3a, and 4a and the peak at 3602 cm^{-1} in Figure 2b, 3b, and 4b, respectively), demonstrating that they possess the highest fraction of intermolecularly associated segments. Note that the free OH peak in the 41 PolyHFS mol % blend with EVA45 is quite small, but present.

It was previously reported[13] that the fragility of intermolecularly hydrogen-bonded polymer blends seems to depend not on the T_g of the blend, but on the fraction of intermolecularly associated segments. Using the association model, it is possible to calculate the theoretical volume fraction of intermolecularly associated segments as a function of composition. Shown in parts a−c of Figure 15 are the blend fragilities and the theoretical volume fraction of intermolecularly associated segments plotted as a function of PolyHFS volume fraction (Φ_B).

As noted previously, the fractions of free and hydrogen-bonded segments determined from the FTIR spectra were calculated at room temperature, and a precise prediction of the volume fraction of intermolecularly associated segments at each blend T_g requires knowledge of the currently unknown enthalpies of hydrogen bonding. Because of the relatively weak hydrogen bonding present in these blends, the hydrogen bonding behavior at each blend T_g should not substantially differ from that determined here. To evaluate

Table 3. VFT Fitting Parameters for the Segmental Relaxations

blend	mol % PolyHFS ± 1%	$\log_{10}[f_0$ (Hz)] ± 1	$B \pm 10$ (K)	$T_o \pm 3$ (°C)	$T_{g,VFT}$ (°C)	fragility ± 10
PVAc	0	12	1710	−14	36	91
	10	11	1400	2	45	100
	24	11	1300	23	64	113
	49	11	930	73	102	179
	74	11	2180	41	109	77
	100	11	1920	63	124	89
EVA70	0	11	1080	−53	−18	97
	13	11	1350	−44	−2	90
	31	11	1130	3	39	121
	58	11	860	62	89	185
	80	10	1830	47	108	83
EVA45	0	11	1010	−64	−33	103
	19	10	920	−44	−13	110
	41	10	930	−12	20	119
	68	10	1890	2	66	68
	86	10	1950	19	83	71

this, dimer and multimer self-association enthalpies of 12 and 4 kJ/mol respectively, were chosen and are slightly less than the self-association enthalpy determined for PVPh self-associations.[37] An intermolecular association enthalpy of 17 kJ/mol was used, and is the same as the enthalpy of intermolecular association determined for blends of PVPh and PVAc.[37] As shown in Figure 16, the hydrogen bonding behavior at each PVAc blend T_g does not appreciably differ from that shown in Figure 6.

The predicted volume fraction of intermolecularly associated segments (black curve in Figure 15a−c) is not meant as a fit of the compositional dependence of the fragility, but rather an indication of which blend compositions should have the highest fragility. For each blend series, the composition closest to the maxima in the prediction line exhibits the highest fragility. This suggests that not only does the fraction of intermolecularly associated segments dictate the fragility in intermolecular hydrogen-bonded polymer blends, but also the Painter−Coleman association model is a useful guide in predicting which compositions should have the highest fragility.

Adam and Gibbs,[38] and recently Stukalin et al.,[39,40] have shown that the fragility is related to the configurational entropy (s_c) and the number of units involved in collective motion (z). As the degree of intermolecular coupling increases, configurational entropy is reduced and z increases. Segmental motion is hindered by intermolecular associations, requiring the breaking of hydrogen bonds before the motion can occur. As temperature approaches the blend T_g, intermolecular associations begin to break, and segmental motion can occur. As temperature increases, hydrogen bond strength decreases,[6] and z will decrease rapidly and the system will gain entropy, s_c, rapidly. It is therefore expected that the compositions with the greatest fraction of intermolecularly coupled segments should have the highest fragility, since the fragility parameter is related to the rate of change of relaxation time with temperature.

As in our previous study of intermolecularly hydrogen-bonded polymer blends,[13] the fragility is not correlated with T_g (see Figure 17).

The highest PolyHFS composition of each series (74, 80, and 86 mol % PolyHFS in the PVAc, EVA70, and EVA45 blends, respectively), as well as the 68 mol % PolyHFS blend with EVA45, exhibits fragilities lower than the neat components. This can be attributed to the effects of plasticization. The addition of 20−30 mol % PVAc (or EVA70, EVA45) to PolyHFS will have a plasticization effect, lowering the fragility of the system, similar to what was shown by Stukalin et al.[40] The 68 and 86 mol % PolyHFS blends with EVA45 both exhibit fragilities lower than PolyHFS because EVA45 has relatively few interacting sites, and should have a stronger plasticizing effect than PVAc or EVA70 due to its higher ethylene content.

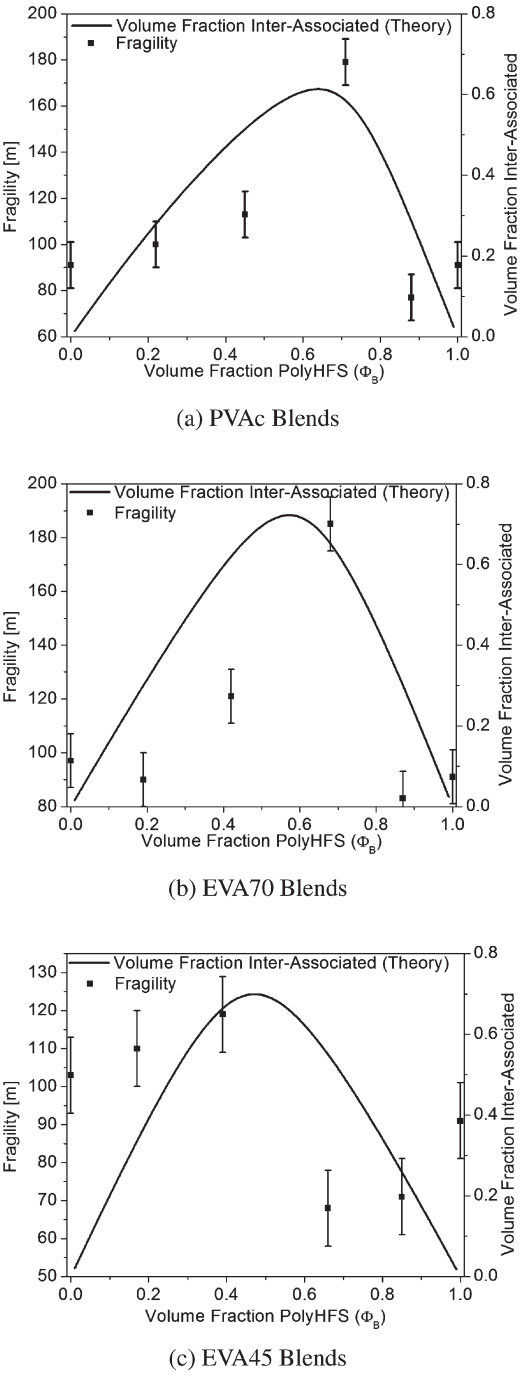

Figure 15. Dynamic fragility (left axes) and the theoretical volume fraction of intermolecularly associated segments (right axes) as a function of PolyHFS composition for (a) PVAc blends, (b) EVA70 blends, and (c) EVA45 blends.

High Temperature Relaxations. At temperatures above and frequencies below the α relaxation, an additional process is present in the dielectric spectrum, α*. Because of the dc conductivity present, this relaxation was most easily observed in the "conductivity-free" (derivative) dielectric loss. An example fit of two derivative HN equations (eq 12) and a power law to this additional process, the segmental relaxation and the onset of electrode polarization is shown in Figure 18.

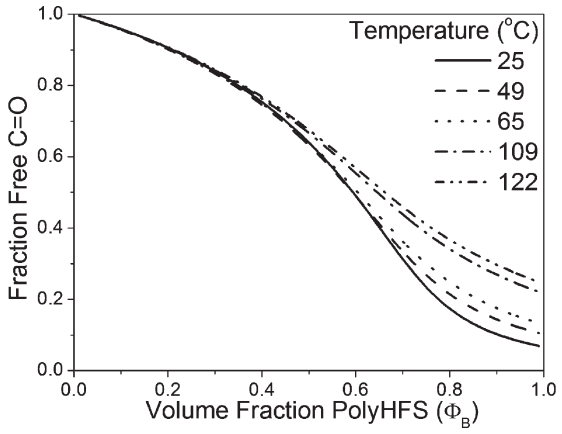

Figure 16. Predicted fraction of free carbonyl groups as a function of composition for PVAc blends at room temperature and the PVAc blend T_g's.

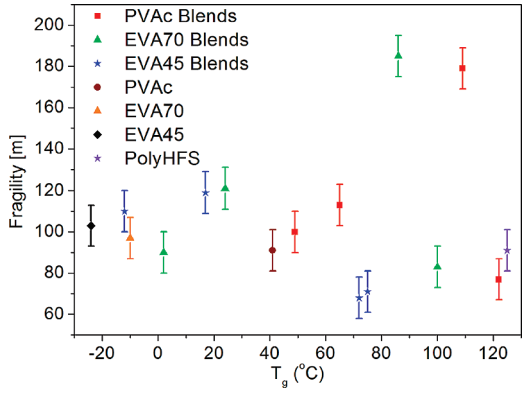

Figure 17. Dynamic fragility as a function of T_g from DSC.

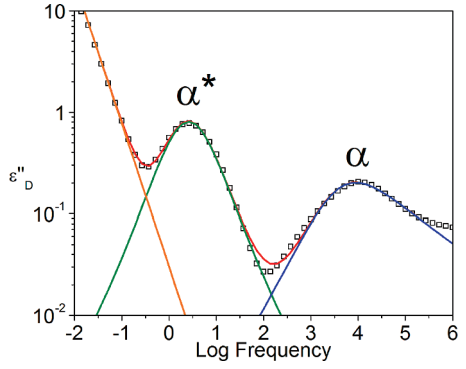

Figure 18. Representative derivative Havriliak−Negami fit to the α* process (green curve) and α process (blue curve) for the 86 mol % PolyHFS blend with EVA45 at 155 °C. The red curve is the sum of two derivative Havriliak−Negami functions and the orange line is a power law to account for the onset of electrode polarization.

Stadler and Freitas,[41] and later Leibler et al.,[42] described the high temperature relaxation behavior of systems where temporary thermoreversible cross-links, or "stickers", exist. Among the predictions of ref 42 is the existence of an additional relaxation process resulting from the breaking and reforming of hydrogen bonds as chains reptate. As the chain reptates (for low sticker contents), associations must be broken for the chain to undergo tube disengagement. Broadband dielectric relaxation spectroscopy monitors dipole motion, and therefore only the response of open stickers can be monitored, since a closed sticker would be expected to have a negligible dipole moment.[29]

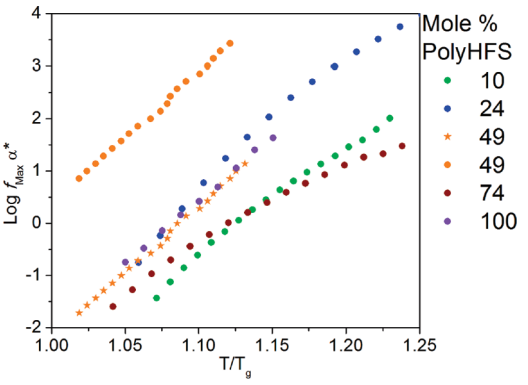

(a) PVAc Blends

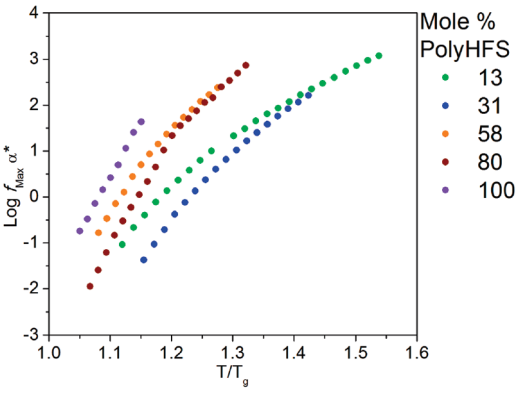

(b) EVA70 Blends

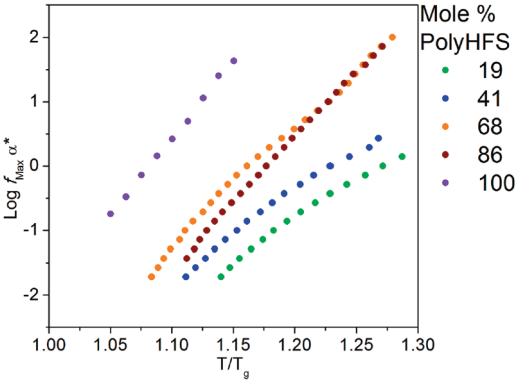

(c) EVA45 Blends

Figure 19. The α* process in the (a) PVAc blends, (b) EVA70 blends, and (c) EVA45 blends versus temperature normalized by T_g.

For each blend, the α* process is nearly Debye ($a = b = 1$), having derivative HN (eq 12) shape parameters $a = 0.8-0.9$ and $b = 1$, which is in agreement with the findings of Wübbenhorst et al.[29] Shown in parts a−c of Figure 19 are the relaxation frequencies of the α* process as a function of temperature normalized by T_g. This process exhibits an Arrhenius (eq 15) temperature dependence over the temperature range investigated, having fit parameters: $f_0 = 10^{27\pm3}$ Hz and $E_a = 150 \pm 60$ kJ/mol. The large uncertainty in activation energies is due to the somewhat VFT-like behavior exhibited by this relaxation in some of the blends, particularly those with EVA70. Wübbenhorst et al.[29] predicted the α* relaxation should exhibit a VFT temperature dependence over a sufficiently broad temperature range, but Müller et al.[43] modeled

this relaxation with an Arrhenius function. The process, does, however, appear to exhibit a VFT-like temperature dependence in another study by Müller et al.[44] Because of the relatively small temperature window over which the relaxation time of this process can be determined, a VFT fit would not be reasonable in many cases here.

Inspection of parts a−c of Figure 19 reveals that as the ethylene content in the blend increases (PVAc < EVA70 < EVA45), the α* relaxation extrapolates to lower frequencies, or higher temperatures, relative to PolyHFS. This suggests that as ethylene content is increased, the α* relaxation becomes more disconnected from the segmental process. This trend is expected, since the ethylene portion does not hydrogen bond, so although miscible, a greater fraction of the blend is unassociated as ethylene content is increased. Unassociated segments can reptate without breaking hydrogen bonds, so relative to T_g, segmental-level motion can occur more readily to higher temperatures in the EVA45 blends than in the EVA70 or PVAc blends before hydrogen bonds must be broken. Every segment in the PVAc blends can hydrogen bond, so at blend compositions where the volume fraction of HFS and VAc segments are approximately equal, segmental level motion cannot occur without breaking hydrogen bonds.

The 49 mol % PolyHFS blend with PVAc exhibits two α* relaxations (orange circles and stars in Figure 18) at temperatures above its segmental process, and is the only blend to do so. One of the relaxations, represented by the stars, occurs at time scales similar to that of PolyHFS when normalized by T_g, and the other process occurs at higher frequencies or lower temperatures. Although not shown here, the relaxation represented by the orange stars in Figure 19a is of lower magnitude ($\Delta\varepsilon$) than the relaxation represented by the orange circles. This blend likely becomes slightly heterogeneous at elevated temperatures, resulting in a hydrogen-bonding relaxation for the HFS homopolymer (orange stars), and a hydrogen bonding relaxation for the PVAc still hydrogen bonded to the HFS homopolymer (orange circles).

Conclusions

The effects of strong intermolecular associations on the dynamics of miscible hydrogen-bonded blends of PolyHFS with PVAc, EVA70, and EVA45 have been investigated. The Painter−Coleman association model, along with careful analysis of the state of hydrogen bonding in the blends allows for predictions of the relative strengths of glassy state relaxations of these systems. Hydrogen bonding couples the local relaxations, and retards the PolyHFS local process.

The fragility of hydrogen-bonded polymer blends is strongly dependent on the fraction of segments that form hydrogen bonds. The association model allows for a prediction of which blend compositions have the highest fragility, and should be applicable to any system where the infrared response can be quantified, or the enthalpies of hydrogen bond formation are known.

A high temperature relaxation related to the breaking and reforming of hydrogen bonds as the chains reptate is present in the blends. As the ethylene content of the blends increases, the relaxation moves to higher temperatures relative to the segmental process, since reptation can proceed more readily in these systems without breaking the intermolecular associations.

Acknowledgment. K.A.M. and J.R. thank the National Science Foundation Polymers Program for financial support of this research through DMR-0605627 and DMR-0907139. P.C.P. and H.Z. thank the National Science Foundation for financial support through DMR-0901180.

References and Notes

(1) Robertson, C. G.; Roland, C. M. *J. Polym. Sci., Part B: Polym. Phys.* **2004**, *42*, 2604–2611.
(2) Painter, P. C.; Veytsman, B.; Kumar, S.; Shenoy, S.; Graf, J. F.; Xu, Y.; Coleman, M. M. *Macromolecules* **1997**, *30*, 932–942.
(3) Lodge, T. P.; McLeish, T. C. B. *Macromolecules* **2000**, *33*, 5278–5284.
(4) Lodge, T. P.; Wood, E. R.; Haley, J. C. *J. Polym. Sci., Part B: Polym. Phys.* **2006**, *44*, 756–763.
(5) Painter, P. C.; Coleman, M. M. *Macromolecules* **2009**, *42*, 820–829.
(6) Coleman, M. M.; Graf, J.; Painter, P. C. *Specific Interactions and the Miscibility of Polymer Blends*, 1st ed.; Technomic Publishing Company: Lancaster, PA, 1991.
(7) Zhang, S. H.; Jin, X.; Painter, P. C.; Runt, J. *Polymer* **2004**, *45*, 3933–3942.
(8) Zhang, S. H.; Painter, P. C.; Runt, J. *Macromolecules* **2004**, *37*, 2636–2642.
(9) Zhang, S. H.; Runt, J. *J. Polym. Sci., Part B: Polym. Phys.* **2004**, *42*, 3405–3415.
(10) Yang, X. M.; Painter, P. C.; Coleman, M. M.; Pearce, E. M.; Kwei, T. K. *Macromolecules* **1992**, *25*, 2156–2165.
(11) Coleman, M. M.; Pehlert, G. J.; Yang, X. M.; Stallman, J. B.; Painter, P. C. *Polymer* **1996**, *37*, 4753–4761.
(12) Pehlert, G. J.; Yang, X. M.; Painter, P. C.; Coleman, M. M. *Polymer* **1996**, *37*, 4763–4771.
(13) Masser, K. A.; Runt, J. *Macromolecules* **2010**, *43*, 6414–6421.
(14) Coleman, M. M.; Pehlert, G. J.; Painter, P. C. *Macromolecules* **1996**, *29*, 6820–6831.
(15) Coleman, M. M.; Painter, P. C. *Prog. Polym. Sci.* **1995**, *20*, 1–59.
(16) Choperena, A.; Painter, P. *Macromolecules* **2009**, *42*, 6159–6165.
(17) Painter, P.; Zhao, H. Q.; Park, Y. *Macromolecules* **2009**, *42*, 435–444.
(18) Gaikwad, A. N.; Choperena, A.; Painter, P. C.; Lodge, T. P. *Macromolecules* **2010**, *43*, 4814–4821.
(19) Cerveny, S.; Alegria, A.; Colmenero, J. *Phys. Rev. E* **2008**, *77*, 0318031–0318035.
(20) Cerveny, S.; Alegria, A.; Colmenero, J. *J. Chem. Phys.* **2008**, *128*, 0449011–0449017.
(21) Smith, G. D.; Liu, F. G.; Devereaux, R. W.; Boyd, R. H. *Macromolecules* **1992**, *25*, 703–708.
(22) Kim, S.; Mundra, M. K.; Roth, C. B.; Torkelson, J. M. *Macromolecules* **2010**, *43*, 5158–5161.
(23) Havriliak, S.; Negami, S. *J. Polym. Sci., Part C: Polym. Symp.* **1966**, 99–117.
(24) Onsager, L. *J. Am. Chem. Soc.* **1936**, *58*, 1486–1493.
(25) Kirkwood, J. G. *J. Chem. Phys.* **1939**, *7*, 911–919.
(26) Kremer, F.; Schonhals, A. *Broadband Dielectric Spectroscopy*, 1st ed.; Springer-Verlag: New York, 2003.
(27) Steeman, P. A. M.; vanTurnhout, J. *Colloid Polym. Sci.* **1997**, *275*, 106–115.
(28) Wübbenhorst, M.; vanKoten, E. M.; Jansen, J. C.; Mijs, W.; vanTurnhout, J. *Macromol. Rapid Commun.* **1997**, *18*, 139–147.
(29) Wübbenhorst, M.; van Turnhout, J.; Folmer, B. J. B.; Sijbesma, R. P.; Meijer, E. W. *IEEE Trans. Dielectr. Electr. Insul.* **2001**, *8*, 365–372.
(30) Wübbenhorst, M.; van Turnhout, J. *J. Non-Cryst. Solids* **2002**, *305*, 40–49.
(31) Fragiadakis, D.; Dou, S.; Colby, R. H.; Runt, J. *J. Chem. Phys.* **2009**, *130*, 0649071–06490711.
(32) Tyagi, M.; Alegria, A.; Colmenero, J. *Phys. Rev. E* **2007**, *75*, 0618051–0618059.
(33) Fragiadakis, D.; Runt, J. *Macromolecules* **2010**, *43*, 1028–1034.
(34) Tyagi, M.; Arbe, A.; Alvarez, F.; Colmenero, J.; Gonzalez, M. A. *J. Chem. Phys.* **2008**, *129*, 2249031–22490314.
(35) Angell, C. A. *Science* **1995**, *267*, 1924–1935.
(36) Richert, R.; Angell, C. A. *J. Chem. Phys.* **1998**, *108*, 9016–9026.
(37) Zhang, S. H.; Painter, P. C.; Runt, J. *Macromolecules* **2002**, *35*, 8478–8487.
(38) Adam, G.; Gibbs, J. H. *J. Chem. Phys.* **1965**, *43*, 139–146.
(39) Stukalin, E. B.; Douglas, J. F.; Freed, K. F. *J. Chem. Phys.* **2009**, *131*, 1149051–11490511.
(40) Stukalin, E. B.; Douglas, J. F.; Freed, K. F. *J. Chem. Phys.* **2010**, *132*, 0845041–08450411.
(41) Stadler, R.; Freitas, L. D. *Macromolecules* **1989**, *22*, 714–719.
(42) Leibler, L.; Rubinstein, M.; Colby, R. H. *Macromolecules* **1991**, *24*, 4701–4707.
(43) Müller, M.; Stadler, R.; Kremer, F.; Williams, G. *Macromolecules* **1995**, *28*, 6942–6949.
(44) Müller, M.; Kremer, F.; Stadler, R.; Fischer, E. W.; Seidel, U. *Colloid Polym. Sci.* **1995**, *273*, 38–46.